Laboratory study of wind loads on a low-rise building in a downburst using a moving pulsed jet simulator and their comparison with other types of simulators

Kazunori ASANO[1*], Yumi IIDA[2] and Yasushi UEMATSU[1]

1 Department of Architecture and Building Science, Tohoku University, Sendai 980-8579, Japan, asano-k@dc.tohoku.ac.jp

2 Technical Research Inst. of Obayashi Corp., Tokyo, Japan, iida.yumi@obayashi.co.jp

* Corresponding author

Abstract

Downburst produces strong winds near the ground and causes severe damage to buildings and people. The non-stationarity of downburst is characterized by moving downdraft and pulsed jet to the ground. In practice, both characteristics have often been observed simultaneously. These characteristics significantly affect the wind loads on buildings, particularly on low-rise buildings. However, the previous experimental studies of downbursts focused on each of these characteristics separately. No study has been made of their coupled effect. Therefore, we have developed a downburst simulator, which can generate a pulsed jet and a moving downdraft either separately or simultaneously. In the present paper, we have experimentally investigated the effects of non-stationary characteristics of downbursts on the wind field and wind loads on a flat-roofed low-rise building using this downburst simulator. The results may become a useful database for validating numerical simulation models of downbursts.

Keywords: Downburst simulator, Non-stationarity, Wind tunnel experiment, Wind velocity, Wind pressure distribution, Wind load.

1 INTRODUCTION

Downbursts produce strong winds near the ground and may cause severe damage to buildings and structures, and occasionally injure people. Therefore, it is important to understand the aerodynamic characteristics of downburst winds near the ground for establishing a rational downburst resistant design of buildings and structures. However, only a few studies have been made of the characteristics of downburst flows near the ground, up to 100 m above the ground, for example, where most buildings and structures exist. Moreover, few studies have been conducted on downburst-induced aerodynamic forces on buildings.

Chay and Letchford [1], Zhang et al. [2, 3], Mason et al. [4], Letchford and Chay [5], Sengupt et al. [6], McConville [7] and Jubayer et al. [8] conducted experiments using impinging jets. Chay and Letchford [1] and Zhang et al [2, 3] discussed the mean wind profile and wind forces acting on buildings of various shapes using a stationary jet that kept blowing at a constant wind speed for the entire duration of the experiment. Mason et al. [4] attached a shutter to the blower to reproduce an instantaneous jet, which is one of the characteristics of downbursts. Letchford and Chay [5] and Sengupt et al. [6] investigated the influence of movement of downdraft on the wind loads on buildings using a movable device. McConville [7] carried out an experiment for reproducing downbursts by using an impinging jet. In order to reproduce the characteristics of moving downdraft, an anemometer was moved along a horizontal line above the floor in the jet flow instead of the use of moving jet. Jubayer et al. [8] examined the difference in the wind pressure distribution and the resultant wind forces on a high-rise building between in a fixed impinging jet and in a turbulent boundary layer. In these studies, focus was on the non-stationarity of downbursts, characterized by either moving downdraft or pulsed jet against the ground. In practice, however, both characteristics are observed simultaneously [9 - 11]. It is important to reproduce both characteristics in the experiment, because both of them may affect the wind loads on buildings and structures significantly, particularly on low-rise buildings, considering the vertical wind velocity profile of downburst.

Based on the above-mentioned discussion, our research group has developed a downburst simulator, which can simulate non-stationery downburst winds appropriately [12]. The present paper discusses the effects of non-stationary characteristics of downbursts on the wind field and wind loads on a flat-roofed low-rise building, based on the experiments with this downburst simulator. The pulsed jet and the moving jet are reproduced either separately or simultaneously. The effect of the combination of these jets is also investigated. First, the characteristics of downburst winds near the ground are investigated. Then, the instantaneous pressure distributions on a flat-roofed low-rise building are measured under various conditions. The results are compared with those obtained from a wind tunnel experiment with the same model in a turbulent boundary layer. Finally, a discussion is made of the design wind loads for downbursts.

2 EXPERIMENTAL APPARATUS AND PROCEDURE

2.1 Downburst Simulator

Fujita et al [13] showed that the pressure increased near the center due to the downdraft from the downburst. Then, the high pressure and the low pressure alternately

occurred in the form of a ring around the high-pressure zone. Fujita estimated that the minimum downburst diameter was at least 400 m. Lin [14] suggested that strong downbursts had downdraft diameters less than 2000 m. Holmes [15] estimated that low-pressure ring radius of AAFB downburst was approximately 1000m. Based on the above discussion, the diameter D of the AAFB downburst is assumed 1200 m. And the geometric scale of the downburst simulator is assumed 1/2000.

Figure 1(a) shows the downburst simulator that we have developed. The simulator blows up to the ceiling board instead of blowing down to the floor, which makes it possible to translate the heavy blower fast and in safety (Figure 1(b)). The diameter (D) of the blower is 600 mm, which is used as a representative length for the normalization in the present paper. The distance H_{blower} between the ceiling board and the outlet of the apparatus is 1000 mm; the ratio of the distance H_{blower} to the diameter D of the blower is 1.67. The blower has a honeycomb and a mesh installed above the fan to reduce the effects of swirl generated by the fan and make the flow uniform. The wind speed of the blower can be controlled by an inverter whose range can be changed from 0 to 60 Hz. The maximum rotation velocity of the fan is 1730 rpm and the air flow rate is approximately 200 m^3/min at 60 Hz.

The downdraft velocity at a position of 100 mm above the blower outlet is set to V_j = 7.17 m/s with a turbulence intensity of 3.1%. In order to reproduce the pulsed jet, a shutter is installed above the outlet of the blower, which makes instantaneous jets by its rapid opening. The duration of opening (shutter opening time) can be changed from 0.2 to 0.3 s. The shutter opening time of 0.2 s is used here based on the results of previous studies [12, 16]. In this case, we can observe a peak wind speed clearly, which corresponds well to the field observation.

(a) Blower with a shutter generating pulsed jet

(b) Rails on which the blower moves

Figure 1. Downburst simulator

A downburst occurs so locally that the running distance is much shorter than that of the ordinary turbulent boundary layer, such as typhoon, for example. It is thought that the profile is minutely affected by the terrain roughness. Therefore, the effect of terrain roughness is not considered in the present study. In practice, the surface of the ceiling board is smooth.

In order to reproduce the movement of downburst with its parent cloud, which is one of the characteristics of downbursts, the blower can move on the rails in the X direction (see Figure 2). The moving speed V_{tr} can be changed from 0.5 to 2 m/s. The change of moving speed in the X direction is schematically illustrated in Figure 3. It moves at a constant speed under the ceiling board. Letchford and Chay mention that the moving speed is as high as 30 % of the downdraft velocity. Since 30 % of V_j = 7.17 m/s is 2.15 m/s, the moving speed is set to V_{tr} = 2 m/s in the present experiment. A sensor that detects the passage of the blower is attached to the rail and the shutter opens instantaneously when the blower passes the location X_0 of this sensor. The position X_0 can be changed within the range of 'constant velocity range' (see Figures 2 and 3).

Figure 4 shows the vertical profiles of mean wind velocity and turbulence intensity for the stationary downburst flow, in which the blower is located at $X_0/D = -1$. The mean wind velocity V_z is measured by a hot wire anemometer installed at various heights, in which V_{max} represents the maximum mean wind velocity in the profile. It can be seen that the mean wind velocity is relatively high near the ground. The mean wind velocity decreases and the turbulence intensity increases with increasing height.

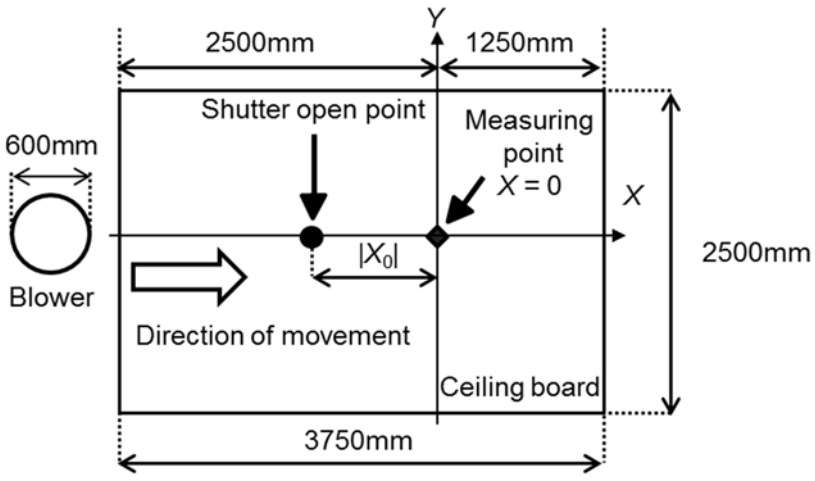

Figure 2. Ceiling board and coordinate system

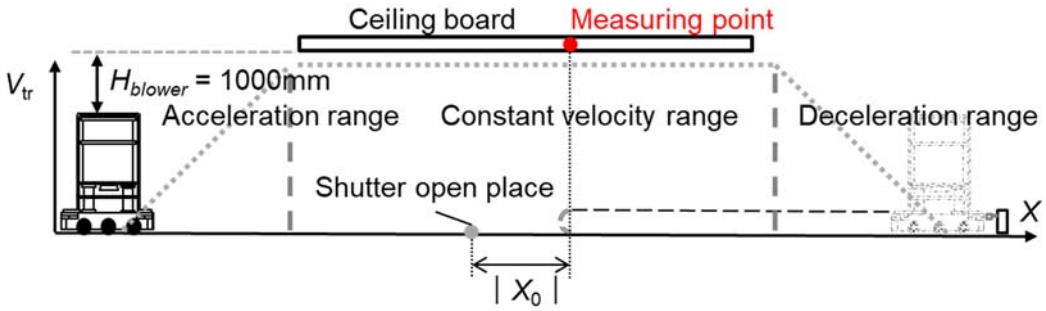

Figure 3. Schematic illustration of the change in moving speed of the blower

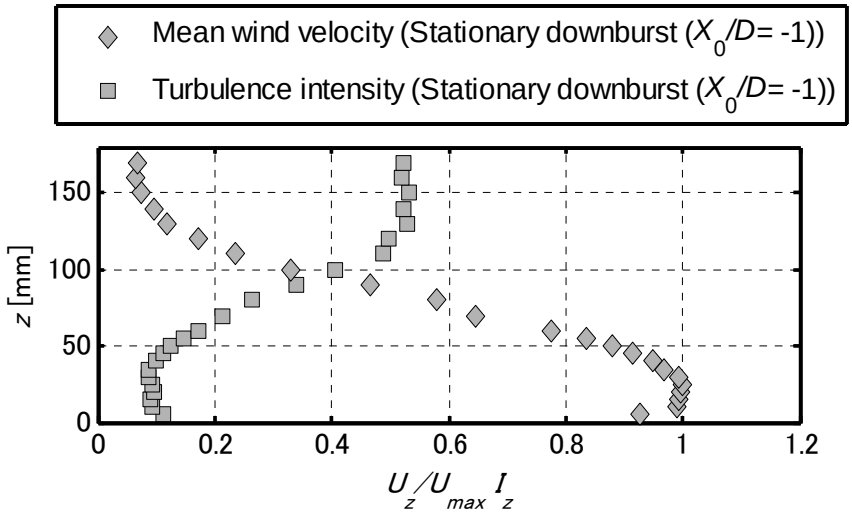

Figure 4. Vertical profiles of mean wind velocity and turbulence intensity in stationary downburst at $X_0/D = -1$.

2.2 Building model and pressure measurements

The model building under consideration in the present study is a flat-roofed low-rise building with width (W) × length (L) × height (H) = 80 m × 80 m × 40 m. The test model is made of acrylic plates with a geometric scale of 1/2000 (Figure 5). Pressure taps of 1 mm diameter are drilled on the walls and roof. The total number of pressure taps is 73, among which 12 pressure taps are installed on each wall and 25 pressure taps on the roof (Figure 6). The pressure taps are connected to pressure transducers (MAPS-02 with capacity of ± 125 mm H_2O and linearity of 0.1% FS at a rate of 800 Hz, Wind Engineering Institute Co., Ltd), in parallel via 1 m lengths of vinyl tubes of 1.5 mm inside diameter. The wind pressures at all pressure taps were sampled simultaneously at a rate of 800 Hz. The distortion of fluctuating wind pressures caused by the tubing system is corrected by using the frequency response function of the measuring system in the frequency domain.

Figure 5. Building model

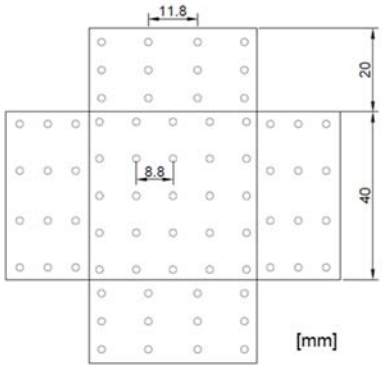

Figure 6. Layout of pressure taps

2.3 Wind Tunnel Experiment with a turbulent boundary layer

Wind tunnel experiment is carried out in the Eiffel type boundary layer wind tunnel at the Department of Architecture and Building Science, Tohoku University, which is 6.5 m in length and 1.0 m × 1.4 m in cross-section. A turbulent boundary layer is generated on the wind tunnel floor using spires and roughness blocks. Figure 7 shows the vertical profiles of the mean wind speed U_Z and the turbulence intensity I_u of the flow. The power law exponent α of the mean wind speed profile is approximately 0.2, which simulates natural winds over typical suburban terrain. The turbulence intensity I_Z at the model height H is approximately 0.22.

The design wind speed is determined based on the AIJ Recommendations for Loads on Buildings [17]. It is assumed that the 'Basic wind speed' is U_0 = 35 m/s and the terrain category is III (α = 0.2, Z_G = 450 m), which corresponds to suburban terrain. The design wind speed U_H at the roof height (reference height, H = 40 m) is calculated as 36.7 m/s. In the experiment, the wind speed at the reference height is set to U_H = 6 m/s. Therefore, the velocity scale is approximately 1/6, resulting in the time scale of 1/327, considering the length scale of 1/2000. Since the evaluation time of wind speed at the meteorological observatories of the Japan Meteorological Agency is 10 min, the evaluation time of the statistics of wind speeds and wind pressures is set to 10 min in full scale, which corresponds to 1.84 s in the model scale. The experiments are repeated 10 times under the same condition. The statistical values of wind speeds and wind pressures are evaluated by applying ensemble average to the results of the 10 consecutive runs.

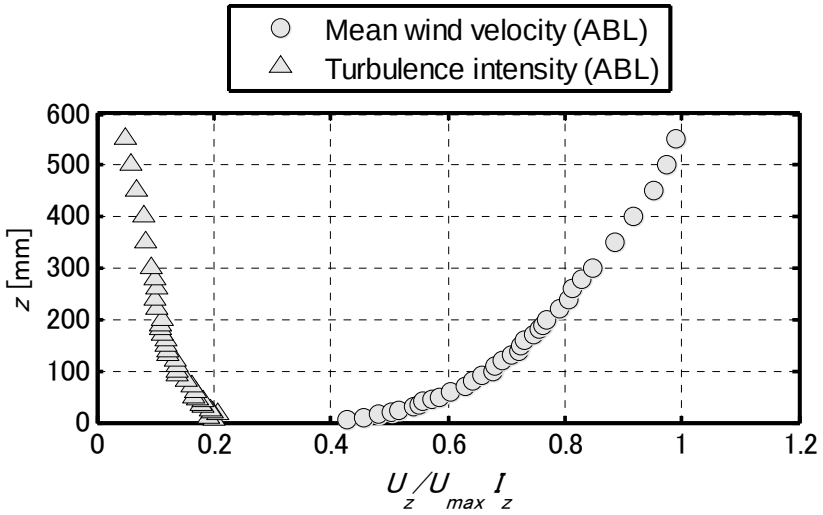

Figure 7. Vertical profiles of dimensionless wind velocity and turbulence intensity of the turbulent boundary layer

3 RESULTS OF DOWNBURST EXPERIMENT

In order to obtain the vertical profiles of wind velocity near the ground and the wind pressures on the building model, the following three kinds of jets are used:

(1) Stationary pulsed jet: this is a stationary pulsed jet generated by opening the shutter instantaneously, in which the blower is located at $X_0/D = -1$.

(2) Moving jet: this is a steady impinging jet moving at a constant speed V_{tr}.

(3) Moving pulsed jet: this is a pulsed jet moving at a constant speed. The shutter opens instantaneously at a predetermined point X_0 while moving.

3.1 Wind Velocity Profile near the Ground

The flow field generated in the present experiment is so complicated that it is difficult to measure all components of wind speed accurately. Therefore, a hot wire anemometer with I-type probe is used to obtain the maximum value of wind speed near the ground. The probe is placed vertically at $X = 0$ (see Figure 2) under the ceiling. The height Z of the probe is changed from 5 to 60 mm at a step of 5 mm and from 70 to 200 mm at a step of 10 mm. The sampling rate of measurements is 1 kHz. The sampling time depends on the experiment. For the stationary pulsed jet, it is set to 30 s, because the wind keeps blowing after the shutter has opened and we don't know when the maximum peak wind speed occurs beforehand. For the moving jet and moving pulsed jet, on the other hand, a sampling time of approximately 10 s is long enough to capture the whole event because the jet passes the measuring point in a short time. Thus, the

sampling time is set to 15 s in these cases.

According to the results of our previous experiments [12, 16], the maximum instantaneous wind velocity occurs when the blower is located at $X_0/D = -1$ in the stationary pulsed jet case. Therefore, the same location of the blower is used in the pulsed jet experiment. In the moving pulsed jet experiment, the jet is generated at seven positions ranging from $X = -600$ to -1800 mm at a step of 200 mm. As a result, 9 types of measurements are conducted; i.e. the moving jet, the stationary pulsed jet with $X_0/D = -1$, and 7 types of moving pulsed jets with different values of X_0/D, i.e. -1, -1.33, -1.67, -2, -2.33, -2.67 and -3).

Hjelmfelt [18] showed the wind velocity profiles of eight full-scale downbursts. Figure 8 shows a comparison between the Hjelmfelt's results and the present results for the moving pulsed jets with $X_0/D = -1$, -2 and -3, the moving jet and the stationary pulsed jet. Regarding the Hjelmfelt's results, the maximum, mean and minimum values of the observation data are plotted in the figure. Here, $V_{z\max}$ represents the maximum wind velocity at height Z, which is non-dimensionalized by the maximum value $V_{\max}$ in each profile. The height Z is non-dimentionalized by the height $Z_{\max}$ providing the maximum velocity V_{max}. It is found that the overall trends are similar to each other. The wind velocities at higher levels are somewhat larger in the moving jet than in the stationary pulsed jet. This is because the moving of the jet affects the velocity field over a wider area below the ceiling board. In the case of the stationary pulsed jet, the maximum value occurs at a height of approximately 15 mm above the ground, and the wind velocity decreases with height significantly. In the case of the moving pulsed jet, the profile significantly changes with X_0. Comparing these results with those in the stationary pulsed jet, the maximum wind velocity of the moving jet occurs at almost the same height. Table 1 summarizes the values of $V_{\max}$, $Z_{\max}$ and $V_{\max}/V_J$ in each experiment. The maximum wind velocity in the moving pulsed jet is almost the same as or slightly larger than that in the stationary pulsed jet. The scatter of the data for the moving pulsed jets is larger than those of the stationary pulsed jet and the moving jet. This may be due to the combination effect of the two highly nonstationary phenomena, i.e. movement of the apparatus and the pulsed jet.

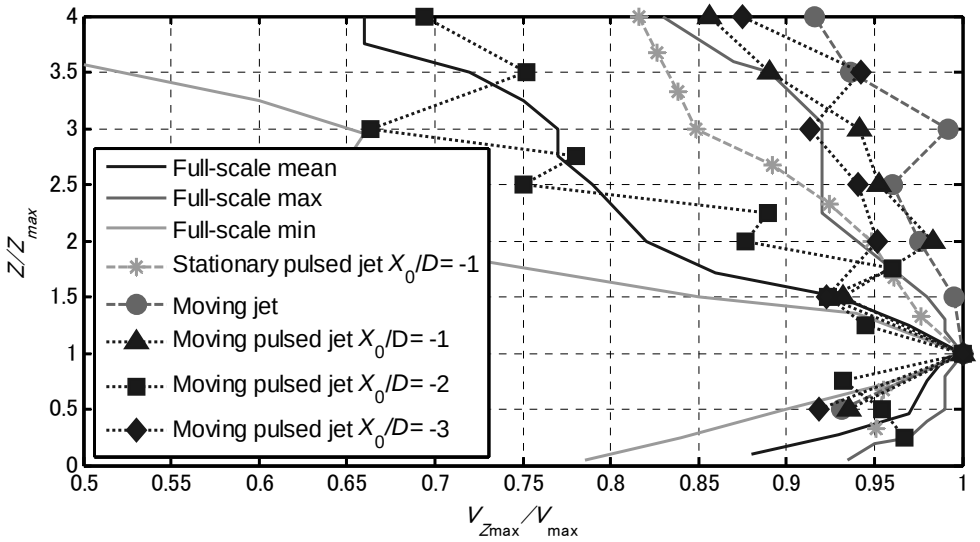

Figure 8. Comparison of non-dimensional velocity profiles between experiments and full-scale measurements by Hjelmfelt [18]

Table 1. The maximum wind velocity and its height for each jet

Flow type	Maximum wind velocity V_{max} (m/s)	Height generating the maximum wind velocity Z_{max} (mm)	V_{max}/V_j
Pulsed jet downburst (X_0/D = –1)	9.84	15	1.38
Moving downburst	11.12	10	1.56
Moving pulsed jet downburst(X_0/D = –2)	10.12	20	1.42
Moving pulsed jet downburst(X_0/D = –3)	11.73	10	1.64

Figure 9 shows the time history of wind velocity at a height of 20 mm (model height) in the case of moving jet (a) and the moving pulsed jet (b, c). The wind velocity V measured by the hot wire anemometer installed at the measuring point (H = 20mm) is non-dimensionalised by downdraft velocity V_j (see Section 2.1).

The results of the ensemble average applied to the results of 10 runs are compared with the observed data for a microburst that hit Andrews Air Force Base (AAFB) near Washington, USA [9]. Note that the observed data are modified so that the maximum value of the non-dimensional wind velocity coincides with that of the experimental data. As mentioned above, the geometric scale is assumed 1/2000 in the present experiment. It seen that both results show a similar trend. The 'downburst eye' can be seen in the simulated downburst in the same manner as in the actual

phenomenon. It is thought that this phenomenon is caused by the moving of the jet. The first peak may be caused by a vortex that occurs when the blower approaches the measuring point. While the blower passes under the measuring point, the flow near the measuring point becomes stagnant, resulting in a low wind velocity. The second peak may be caused by a vortex that occurs when the blower is moving away from the measuring point. The rise time of gust observed in the moving jet is consistent with the practical one. On the other hand, the rise time of gust in the moving pulsed jet is shorter than the practical one. This may be due to the combination of movement and pulsed jet. The rise time of gust is shorter in the case of $X_0/D = -2$ than in the case of $X_0/D = -3$. This feature means that the rise time is dependent on X_0/D significantly.

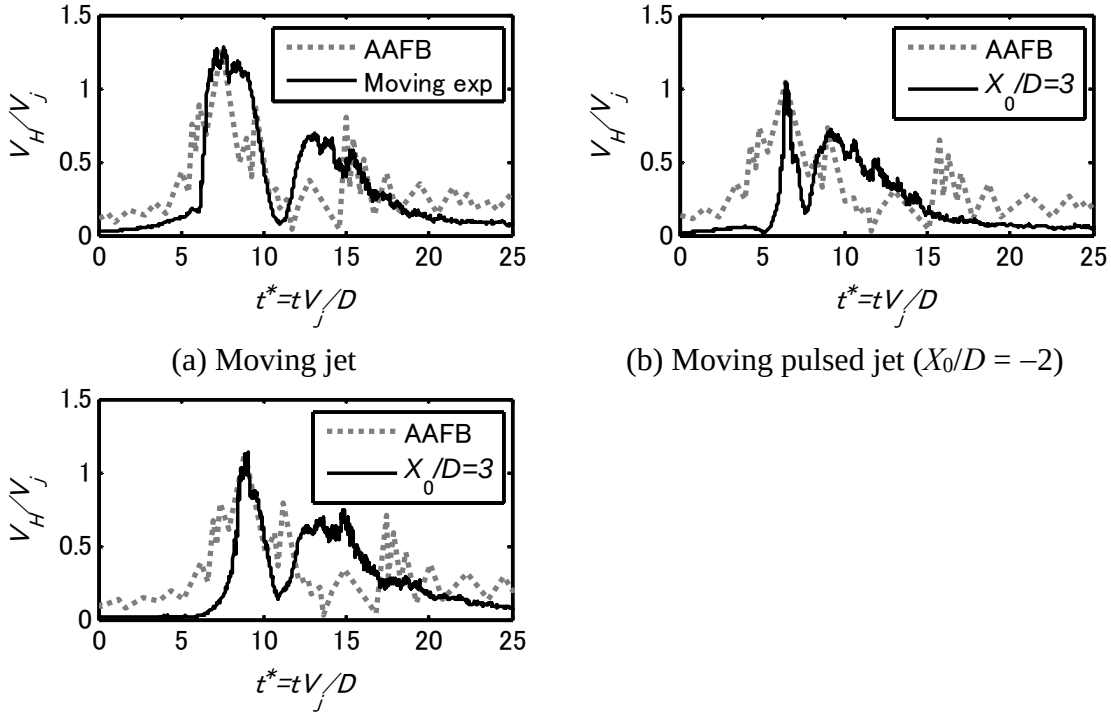

(a) Moving jet

(b) Moving pulsed jet ($X_0/D = -2$)

(c) Moving pulsed jet ($X_0/D = -3$)

Figure 9. Dimensionless time history of velocity at a height of 20 mm compared with the observation data for the AAFB microburst

3.2 Wind Pressures and Forces on a Flat-roofed Low-rise Building

Wind pressures are measured with a building model shown in Figure 5. Differential pressures relative to the atmospheric pressure p_s in the laboratory at a position where the atmospheric pressure is not affected by the downburst simulator are recorded. The pressure time-series are smoothed by using a two-point moving average, which corresponds to an average time of approximately 1 s in full scale.

It is assumed that the wind velocity at the roof height H is approximately 35 m/s in full scale. Therefore, the velocity scale is approximately 1/5, resulting in the time scale of approximately 1/400 considering the geometric scale of 1/2000. According to the previous study by Hjelmfelt [18], the mean duration time of downburst is approximately 13 minutes, which corresponds to approximately 1.95 s in the model scale. Therefore, the measuring time is set to be longer than 2 s for each run.

The model is installed on the ceiling upside down at a location of (X = 0, Y = 0). The model setting angle θ, which corresponds to the wind direction, and the local coordinate system (x, y, z) fixed to the building are defined as shown in Figure 10, where θ = 0° represents a wind direction normal to a wall. The angle θ is changed from 0 to 45° at a step of 15° by rotating the model. The pressure p acting on the model is normalized as the wind pressure coefficient C_p as follows:

$$C_p = \frac{p - p_s}{\hat{q}_H} \tag{1}$$

where p_s = reference static pressure; $\hat{q}_H$ = reference velocity pressure $= 1/2 * \rho V_{H\max}^2$;

$V_{H\max}$ = maximum instantaneous wind velocity with a moving average of 1 s in full scale at the reference point (X = 0 mm and Z = 20 mm) without model; and ρ = air density. Because downburst is a non-stationary phenomenon, we cannot define the mean wind velocity like in the turbulent boundary layer case. Thus, the wind pressure coefficient C_p is defined in terms of the maximum instantaneous wind velocity $V_{H\max}$, which is measured by a hot wire anemometer installed at the reference point without the model.

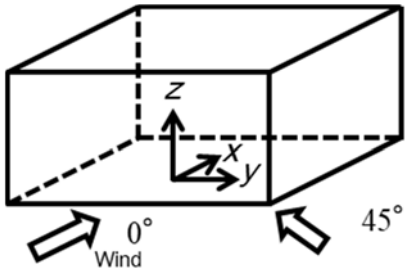

Figure 10. Model setting angle and local coordinate system

The wind-induced forces, F_x, F_y, and F_z, in the x, y and z directions are calculated from the pressure distributions on the walls and roof. Note that the internal pressure is not considered in the calculation of F_z. These wind forces are normalized as wind force

coefficients defined by the following equations:

$$C_{Fx} = \frac{F_x}{\hat{q}_H \cdot B \cdot H} \tag{2–1}$$

$$C_{Fy} = \frac{F_y}{\hat{q}_H \cdot L \cdot H} \tag{2–2}$$

$$C_{Fz} = \frac{F_z}{\hat{q}_H \cdot B \cdot L} \tag{2–3}$$

In order to compare the results in the ABL with those in the downburst, the pressure p acting on the model in the ABL experiment is normalized as the wind pressure coefficient C_{p^*} as follows:

$$C_{p^*} = \frac{p^* - p^*_s}{\hat{q}^*_H} \tag{3}$$

where p^*_s = reference static pressure in the wind tunnel; $\hat{q}^*_H = 1/2 * \rho \hat{U}^{*2}_H$ = reference velocity pressure; $\hat{U}^*_H$ = reference wind speed at the model height (20 mm) reduced to the 1 s average wind speed by using the Durst curve [19]; and ρ = air density. Both in the downburst and ABL experiments, a moving average is applied to the time history of wind pressures using two consecutive data. Due to the difference in the time scale between the downburst and ABL experiments, the corresponding average time is somewhat different from each other. In practice, the value of average time is approximately 1 s in the downburst experiment, while it is approximately 0.8 s in the ABL experiment.

Figures 11 (a) and 11 (b) respectively show the variation of the maximum and minimum values of C_{Fx} and C_{Fz_roof} with X_0/D when $\theta = 0°$. In the figure, the results of stationary pulsed jet and moving jet are also shown for a comparative purpose. In the moving pulsed jet, the maximum value of $C_{Fx\max}$ is 1.45, which is observed when $X_0/D = -2$. When $X_0/D < -2$, the values of $C_{Fx\max}$ are almost constant regardless of X_0/D, nearly equal to that in the moving jet. It is clear that the largest value of $C_{Fx\max}$ is generated by the moving pulsed jet when the jet occurs at some critical position. Table 2 summarizes the maximum $C_{Fx\max}$ values, the reference velocity pressures $\hat{q}_H$, and the wind force $F_{x\max}$ for the three types of downbursts. The stationary pulsed jet generates the smallest reference pressure $\hat{q}_H$ among the three kinds of jets. Although both wind force coefficients C_{Fx} and C_{Fz_roof} are large in the stationary pulsed jet, the actual wind

forces acting on the building model are smaller than those in the other jets, because the reference velocity pressure is relatively small. The downburst flow by moving pulsed jet produces larger wind forces than those of the moving jet and the stationary pulsed jet. Thus, it is important to consider the combination of the moving and the pulsed jet for evaluating the downburst-induced wind loads on buildings. Figure 11(b) indicates that the influence of X_0/D on $C_{Fz\_roof\max}$ is smaller than that on $C_{Fx\max}$. On the other hand, the $C_{Fz\_roof\min}$ value is affected by X_0/D significantly. This is because the pulsed jet hits the roof surface directly when it passes over the model.

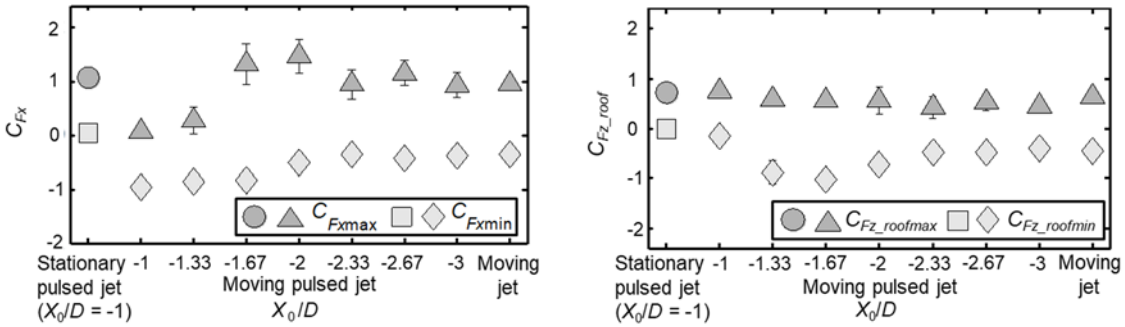

(a) C_{Fx} (θ = 0°) (b) C_{Fz_roof} (θ = 0°)

Figure 11. Variation of wind force coefficients, C_{Fx} and C_{Fz_roof}, with X_0/D

Table 2. Maximum wind force coefficients $C_{Fx\max}$ and reference velocity pressure

	Pulsed jet downburst (X_0/D = –1)	Moving downburst	Pulsed moving downburst (X_0/D = –2)	Pulsed moving downburst (X_0/D = –3)
q_H (H = 20 mm) (N)	50.95	66.51	57.54	70.49
$C_{Fx\max}$	1.05	0.94	1.42	0.92
$F_{x\max}$ (N) (θ = 0°)	53.14	62.54	81.64	63.24
$C_{Fz\_roof\min}$	–0.01	–0.42	–0.71	–0.39
$F_{z\_roof\min}$(N) (θ = 0°)	–0.59	–30.20	–40.87	–27.76

Figure 12 shows the distributions of the minimum peak pressure coefficients, expressed as the development view, when θ = 0°. Shown in Figures 13 is the distribution of the minimum peak pressure coefficients along the centerline of the model, with the windward face being between points 0 and 1, the roof between points 1 and 2 and the leeward wall between points 2 and 3. Because there are no measuring points on the centerline of the wall, the value on the wall surface is provided by the average of the

values at two measuring points near the centerline at the same height. It is found that the minimum peak pressure coefficients generated by downbursts are generally larger in magnitude than those in the ABL. The downbursts tend to generate larger negative pressures on the roof near the windward edge and in the central part compared with the ABL. The stationary pulsed jet generates the minimum peak pressure coefficients, the magnitude of which is larger than twice the value in the ABL. This feature may be due to the generation of vortices caused by the non-stationary pulsed jet. In particular, much larger negative peak pressures are induced in the stationary pulsed jet, the moving jet and the moving pulsed jet with X_0/D = −1 and −1.33. The area of large negative pressures is wider than that in the ABL.

Figure 14 shows the distributions of the minimum peak pressure coefficients, expressed as the development view, when θ = 45°. It is well accepted that, in such a diagonal wind, conical vortices are generated near the windward roof corner in the ABL, which generates large negative peak pressures in this area. Conical vortices are also induced in the downburst experiment. The negative peak pressures are generally larger in magnitude that those in the ABL, except for the moving pulsed jet with X_0/D = −1.67. It is thought that the conical vortices are strengthened by the non-stationarity caused by the pulsed jet and the moving, resulting in larger negative peak pressures.

Figure 15 shows the distributions of the maximum peak pressure coefficients expressed as the development view, when θ = 0°. In addition, Figure 16 shows the distribution of the maximum peak pressure coefficients along the center line of the building. In the figures, the results obtained in the turbulent boundary layer (ABL) are also shown for a comparative purpose. Larger positive pressures are generated on the roof in the case of the moving jet and the moving pulsed jet than in the ABL. This is due to the moving of the blower. When the blower passes under the model, the wind is blowing against the roof directly, generating larger positive peak pressures. Larger positive peak pressures are also generated on the wall. This is due to an increase in wind velocity in the downburst. In the case of the moving pulsed jet, when $X_0/D \geqq -2$, especially at X_0/D = −1.67, large positive pressures are generated in lower area of the wall. This implies that the wind velocities at lower levels are increased in the moving pulsed jet. In particular, it is strongly affected by the wake flow in the cases of X_0/D = −1 and −1.33.

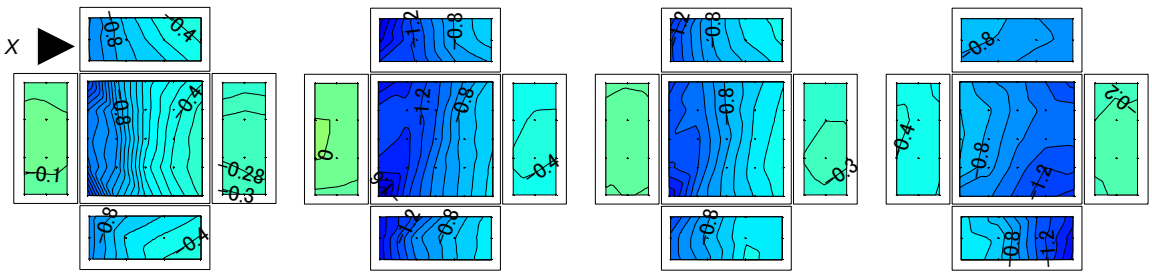

(a) ABL (b) Stationary pulsed jet (c) Moving jet (d) X_0/D = –1

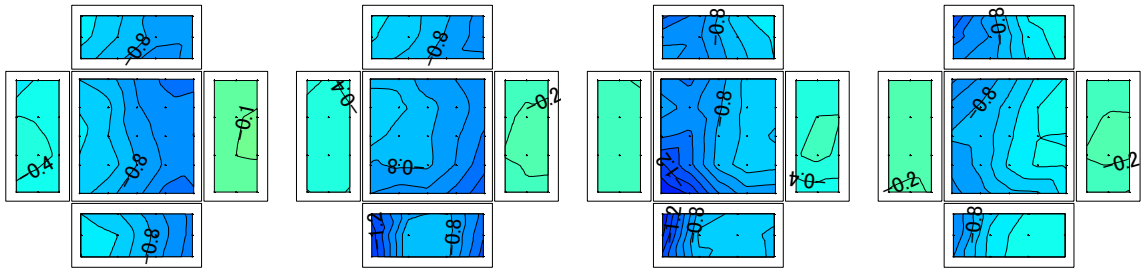

(e) X_0/D = –1.33 (f) X_0/D = –1.67 (g) X_0/D = –2 (h) X_0/D = –3

Figure 12. Distribution of the minimum peak wind pressure coefficients (θ=0°)
((d) – (h) are the results in the moving pulsed jet for various values of X_0/D.)

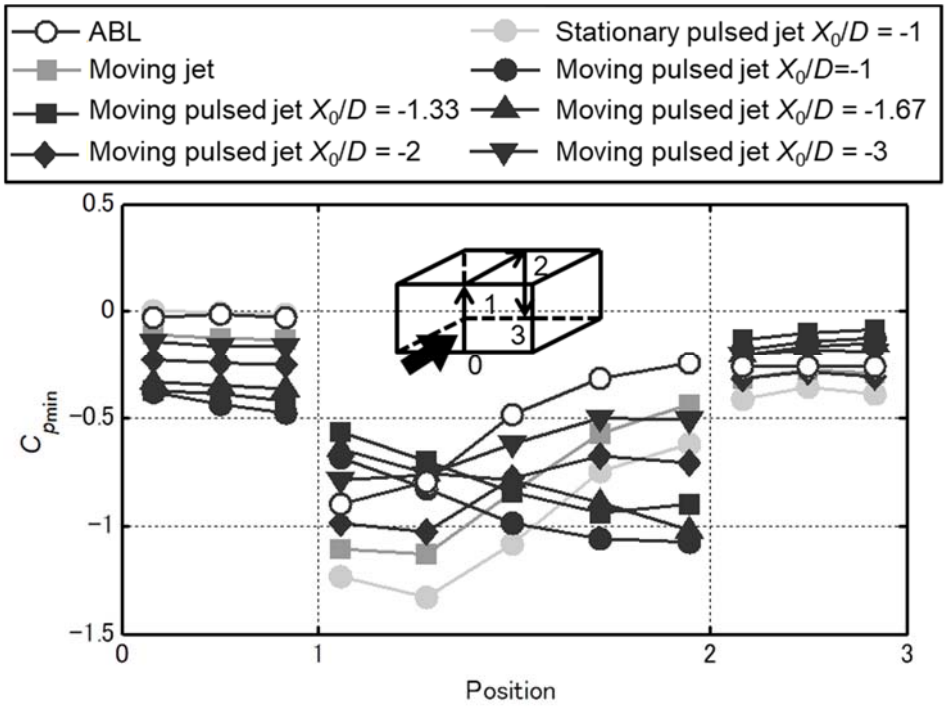

Figure 13. The minimum peak pressure coefficient along the center line of the building

5

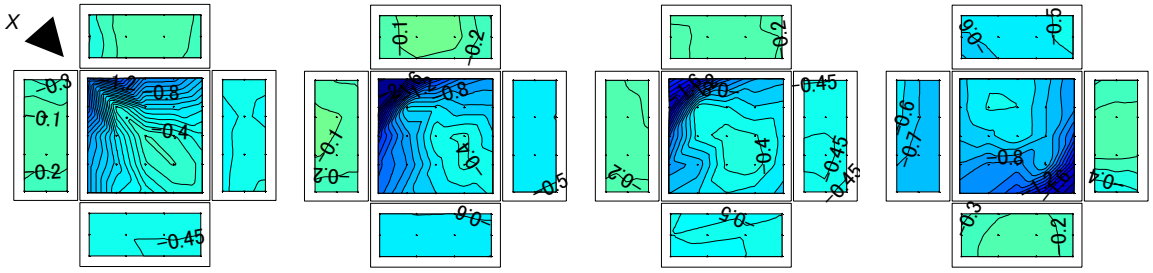

(a) ABL (b) Stationary pulsed jet (c) Moving jet (d) X_0/D = –1

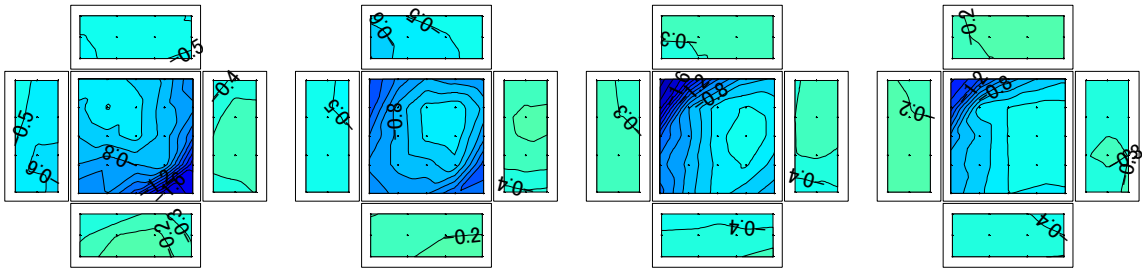

(e) X_0/D = –1.33 (f) X_0/D = –1.67 (g) X_0/D = –2 (h) X_0/D = –3

Figure 14. Distribution of the minimum peak wind pressure coefficients (θ = 45°)
((d) – (h) are the results in the moving pulsed jet for various values of X_0/D.)

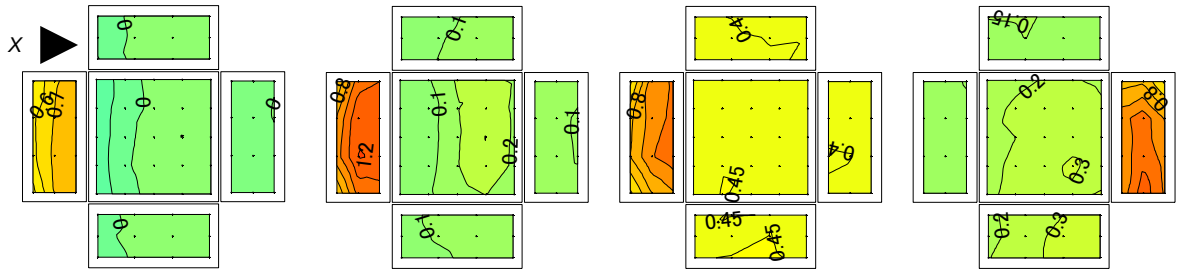

(a) ABL (b) Stationary pulsed jet (c) Moving jet (d) X_0/D = –1

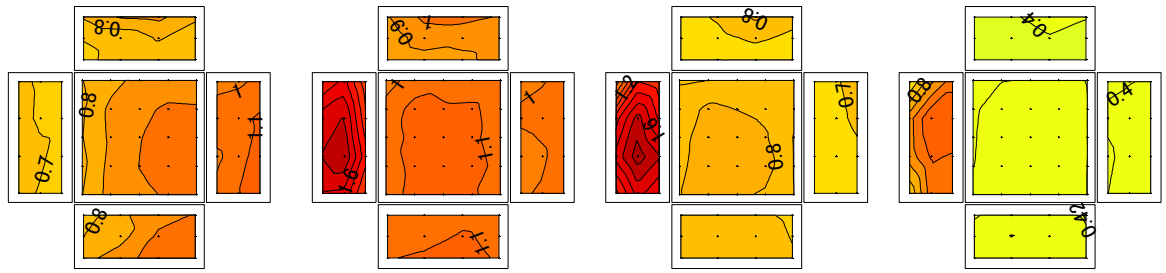

(e) X_0/D = –1.33 (f) X_0/D = –1.67 (g) X_0/D = –2 (h) X_0/D = –3

Figure 15. Distribution of the maximum peak wind pressure coefficients (θ = 0°)
((d) – (h) are the results in the moving pulsed jet for various values of X_0D)

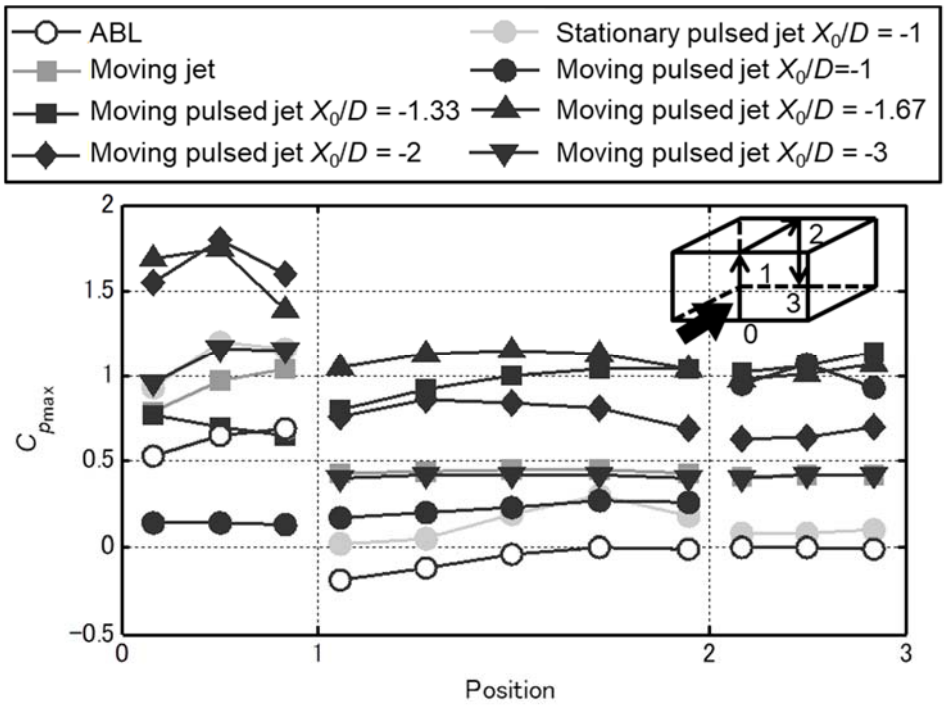

Figure 16. The maximum peak pressure coefficient along the center line of the building

4 CONCLUDING REMARKS

Three types of downbursts, i.e. pulsed jet, moving jet and moving pulsed jet, have been reproduced by using a downburst simulator that we have developed. By moving the blower horizontally, we can reproduce the ‘eye of downburst’, which is a typical characteristic of downbursts. Furthermore, combining the pulsed jet with the moving jet, we can understand the effects of various factors on the flow field of downbursts. In the experiments, the vertical profiles of the maximum instantaneous wind velocities and the time history of wind velocity were obtained. The results were compared with those of field measurements. Both results were consistent with each other not only qualitatively but also quantitatively. The moving of pulsed jet makes the rising time of wind velocity near the ground shorter than the stationary pulsed jet.

The wind pressure distributions on a flat-roofed low-rise building with a square plan were measured in the above-mentioned three types of jets and compared with those obtained in a turbulent boundary layer. Significant differences between them were observed. It is found that the pulsed jet with or without moving produces larger negative pressures on the roof and larger positive pressures on the wall than the turbulent boundary layer. The areas of larger negative and positive pressures are wider than those in the turbulent boundary layer. In the diagonal winds, conical vortices are generated in the turbulent boundary layer. In the pulsed jet, the conical vortices may be

strengthened by the non-stationarity, generating larger negative peak pressures.

The results obtained in the present study indicate that the current wind resistant design of buildings cannot be applied to the downburst resistant design. Further studies are necessary to understand the characteristics of flow field and wind loads on buildings induced by downbursts in more detail. Furthermore, the effect of air temperature on them should be investigated, in which CFD analysis will be investigate turbulent boundary layer,

ACKNOWLEDGEMENT

The present study was financially supported by the JSPS Grants-in-Aid (Grant number 15H0407, FY: 2015 – 2017) for scientific research expenses and The Kajima Foundation (FY: 2013 - 2014).

REFERENCES

[1] M.T. Chay, C.W. Letchford: Pressure distributions on a cube in a simulated thunderstorm downburst Part A: stationary downburst observations, *Journal of Wind Engineering and Industrial Aerodynamics*, Vol. 90, pp. 711-732, 2002

[2] Y. Zhang, H. Hu, Sarkar, P.P.: Modeling of microburst outflows using impinging jet and cooling source approaches and their comparison, *Engineering Structures*, Vol. 56, pp. 779-793, 2013

[3] Y. Zhang, H. Hu, Sarkar, P.P.: Comparison of microburst-wind loads on low-rise structures of various geometric shapes. *Journal of Wind Engineering and Industrial Aerodynamics.* Vol. 133, pp181-190, 2014

[4] M.S. Mason, C.W. Letchford, D.L. James: Pulsed wall jet simulation of a stationary thunderstorm downburst, Part A: Physical structure and flow field characterization, *Journal of Wind Engineering and Industrial Aerodynamics*, Vol. 93, pp. 557-580, 2005

[5] C.W. Letchford, M.T. Chay: Pressure distributions on a cube in a simulated thunderstorm downburst - Part B: moving downburst observations, *Journal of Wind Engineering and Industrial Aerodynamics*, Vol. 90, pp. 733-753, 2002

[6] A. Sengupta, F.L. Hann, P.P. Sarkar, V. Balaramudu: Transient loads on buildings in microburst and tornado winds, *Journal of Wind Engineering and Industrial Aerodynamics*, Vol .96, pp. 2173-2187.

[7] A.C. McConville: The physical simulation of thunderstorm downbursts using an impinging jet, *Wind and Structures*, Vol. 12, No. 2, pp. 133-149, 2009

[8] C. Jubayer, R. Djordje. H. Hangan. Effect of a large scale impinging jet on a

standard tall building. 7th European-African Conference on Wind Engineering, Liege, Belgium, July 5, 2017

[9] T.T. Fujita: Andrews AFB Microburst, SMRP Research Paper 205, University of Chicago, 1983

[10] T.T. Fujita: Tornadoes and downbursts in the context of generalized planetary scales. *Journal of Atmospheric Sciences*, Vol, 38, pp. 1511-1534, 1981

[11] L. Järvi, A. J. Punkka, D. M. Schultz, T. Petäjä, H. Hohti, J. Rinne, T. Pohja, M. Kulmala, P. Hari, T. Vesala: Micrometeorological observations of a microburst in southern Finland, *Boundary-Layer Meteorology.* Vol. 125, Issue 2, pp.343–359 2007

[12] Y. Iida, Y. Uematsu, E. Gavanski: A study of downburst-induced wind loading on buildings, *Journal of Wind Engineering*, JAWE. Vol. 40, No. 2, pp. 40-49, 2015 (in Japanese)

[13] T.T. Fujita: The Downburst, Microburst and Macroburst. SMRP Research Paper 210, University of Chicago, 1985

[14] Lin, W.E.: Validation of a Novel Downdraft Outflow Simulator: A Slot Jet Wind Tunnel, The School of Graduate and Postdoctoral Studies. The University of Western Ontario, Ontario, 2010

[15]J.D. Holmes, S.E. Oliver: An empirical model of downburst, *Engineering Structures*, Vol. 20, pp. 1167-1172, 2000

[16] N.Hoshino, Y. Iida, Y. Uematsu: Effects of non-stationary of downburst on the wind loading of buildings, *Journal of Wind Engineering*, JAWE Vol. 43(1), pp. 1-13, 2018 (in Japanese)

[17] Architectural Institute of Japan: *Recommendations for Loads on Buildings*, 2015 (in Japanese)

[18] M.R. Hjelmfelt: Structure and life cycle of microburst outflows observed in Colorado, *Journal of Applied Meteorology*, Vol. 27, pp. 900-927, 1988

[19] American Society of Civil Engineers: *Minimum design loads for buildings and other structures*, 7-10, third printing, 2013